The influence of the stacking sequence on the electronic structure and optical properties of $CaSi_2$

1997 J. Phys.: Condens. Matter 9 10159

(http://iopscience.iop.org/0953-8984/9/46/014)

J. Phys.: Condens. Matter **9** (1997) 10159–10171. Printed in the UK PII: S0953-8984(97)83390-5

The influence of the stacking sequence on the electronic structure and optical properties of $CaSi_2$

Erkin Kulatov†‖, Hiroshi Nakayama‡ and Hitoshi Ohta§

† The Graduate School of Science and Technology, Kobe University, Rokkodai, Nada, Kobe 657, Japan

‡ Department of Electrical and Electronics Engineering, Faculty of Engineering, Kobe University, Rokkodai, Nada, Kobe 657, Japan

§ Department of Physics, Faculty of Science, Kobe University, Rokkodai, Nada, Kobe 657, Japan

Received 14 April 1997, in final form 12 August 1997

Abstract. The electronic structure and optical properties of $CaSi_2$ have been studied by the *ab initio* full-potential and full-relativistic LMTO methods. Calculations are employed to elucidate the influence of the stacking sequence on the band states and optical spectra. Unusually strong hybridization of the Ca spd states with the Si p states is evident in both of the crystal polymorphs. The Fermi velocities and charge-density distributions indicate significant spatial anisotropy in the TR3 structure. For both of the crystal structures, large in-plane and out-of-plane anisotropy of the optical conductivity has also been found.

1. Introduction

Silicon-based low-dimensional materials are new and promising materials for photonics applications. Various types of Si-skeleton materials have been proposed by Takeda and Shiraishi [1] on the basis of a first-principles local density functional calculation. It was shown that a chainlike Si-skeleton material, SiH_2, reveals a direct band gap of 4 eV and also that a planar material (planar polysilane) shows an intermediate nature between those of the chainlike structure and bulk Si. Planar Si shows an indirect band gap of 2.48 eV and the direct band gap of 2.68 eV. Siloxene ($Si_6O_3H_6$) and its derivatives are well known to show energy gaps corresponding to visible luminescence [2]. On the other hand, the calcium disilicide compound, $CaSi_2$, is known to be a source material for siloxene. $CaSi_2$ has alternating Ca and corrugated Si(111) planes. The Ca layer can be chemically removed by reaction with HCl solution, leaving stacked Si(111) planes.

Siloxene is formed from stacked Si(111) planes which capture H or OH at dangling bonds. Control of the reaction mechanism of HCl solution and $CaSi_2$ is quite important if one is to get the expected composition of siloxene and to avoid further oxidation of the siloxene [3]. Recently, we have studied the change in valence electron states of Ca and Si in $CaSi_2$ subjected to reaction with H_2O by using Auger valence electron spectroscopy [4, 5]. The results showed clearly changes in the valence electron states of Ca and Si caused by the oxidation processes of both the Si and Ca layers during the reaction with H_2O. The two-dimensional nature of the atomic structure of $CaSi_2$ is also an interesting subject within

‖ Author to whom any correspondence should be addressed. Permanent address: General Physics Institute, Russian Academy of Sciences, Vavilov Street 38, 117942, Moscow, Russia; e-mail: kulatov@gimmick.gpi.ac.ru.

0953-8984/97/4610159+13$19.50

solid-state physics. Both theoretical and experimental studies of the electronic structures have been carried out [6–8]. The most important results of these studies are the presence of Ca d electrons and their key role in forming the layer structure of $CaSi_2$. However, the correlations of the two-dimensional atomic structure of $CaSi_2$ with the electronic and optical properties are not clearly revealed or understood.

Keeping these issues in mind, in this paper we present results of *ab initio* band-structure calculations for calcium disilicide, including results for the calculated optical spectra. The point aim of this paper is to present a comparative band-structure study of two calcium disilicide forms, to present their calculated optical properties, and to clarify the role of the stacking sequence as regards the electronic properties. It should be pointed out that the band structure of $CaSi_2$ discussed herein has been investigated by other authors [8–10].

2. The crystal structure of calcium disilicide

The crystal structure of $CaSi_2$ is described by the space group $R\bar{3}m$ (D^5_{3d}, No 166 in the *International Tables of Crystallography*) with the atoms at the following special positions (in the hexagonal classification):

$(0, 0, 0)$, $(2/3, 1/3, 1/3)$, $(1/3, 2/3, 2/3)$ + three atoms in positions 3a: $(0, 0, 0)$
+ six atoms in positions 6c: $(0, 0, z)$, $(0, 0, \bar{z})$.

This structure can be regarded as that of a strongly two-dimensional compound with a layer-by-layer alternate stacking sequence of hexagonal Si bilayers and Ca monolayers along the [0001] hexagonal crystal axis. Recently, several authors have reported the growth of three polymorphs of $CaSi_2$ [11–13], two of which (TR6 and TR3—this notation is from [8], meaning, perhaps, trigonal with six formula units per cell and trigonal with three formula units per cell, respectively) differ only in their stacking sequences and are almost identical in total structural energy [8].

In the TR6 structure the hexagonal unit cell contains six Ca atoms in equivalent positions 6c with $z = 0.083$, six Si atoms in positions 6c with $z = 0.183$ and six Si atoms in positions 6c with $z = 0.350$ [12]. So there are two inequivalent Si atoms, and the stacking sequence is of AABBCC type.

For the TR3 structure, the Ca atoms are coordinated in positions 3a and the Si atoms in positions 6c with $z = 0.197$ [11]. The Ca atoms are shifted by the vector $(2/3, 1/3, 1/3)$ with respect to each other, so no short Ca–Ca distances along the c-axis exist. This structure has an ABC stacking sequence, a three-Ca-layer repeat distance, and eightfold coordination of Ca atoms with Si nearest neighbours.

The third structure with a tetragonal structure [12] does not exist at ambient pressure and we will not consider it here. Instead, for the comparative study we have chosen the H1 (hexagonal with one formula unit per cell) structure which has a very simple AA stacking sequence of alternating Ca layers and Si bilayers. This structure is characterized by a hexagonal unit cell with one Ca atom at position $(0, 0, 0)$ and two Si atoms at positions $(2/3, 1/3, z)$ and $(1/3, 2/3, \bar{z})$, and has not been observed experimentally. The lattice constants, a and c, and the separation between the Ca layers have been taken as those of the TR3 structure. This choice implies that for the H1 structure we need to use the supercell with three formula units. In accordance with the above-mentioned notation, this is the H3 structure.

A general overview of TR6, TR3 and H1 structures can be found in reference [5] and reference [8] (see figure 1 in the latter reference).

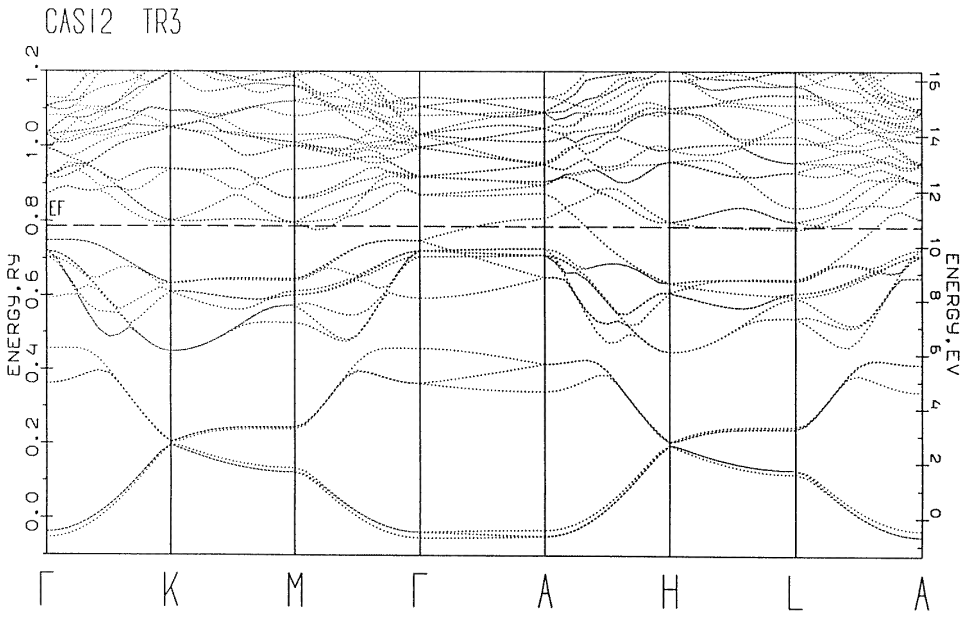

Figure 1. The band structure of TR3-structure $CaSi_2$ along the high-symmetry lines of the hexagonal Brillouin zone. The dashed horizontal line denotes E_F.

3. Details of the calculation

The electronic structure calculations for the TR3 and H3 forms of calcium disilicide were carried out by using the *ab initio* full-potential linear muffin-tin orbitals (FPLMTO) method [14, 15] with plane-wave expansions for the LMTOs in the interstitial region. Exchange and correlation contributions to the crystalline potential have been included through the von Barth–Hedin local density approximation (LDA) [16] to the density functional theory [17, 18]. Here we consider what electronic changes occur as the stacking sequence of the Ca and Si layers is varied. The FPLMTO technique is ideally suited to such kinds of problem, because we generate the electronic structure, spatial charge distribution and chemical bonding of the compound in a completely unified way, i.e. without making any prior assumptions or using any adjustable parameters. In the FPLMTO method the space is divided into touching MT spheres (R_{MT}) surrounding each atom and the remaining interstitial region (Ω_{int}). Within the MT spheres the wave functions are represented in terms of numerical solutions of the radial Schrödinger equation for the spherical part of the potential multiplied by spherical harmonics, as well as their energy derivatives taken at a certain set of energies E_ν that are not yet fixed. In the interstitial region, the wave functions are spherical waves, namely the Hankel functions, taken as the solutions of the Helmholtz equation with a certain fixed value of the average kinetic energy $E = \kappa_\nu^2$. For calculation of the interstitial Hamiltonian matrix elements and representation of the charge density, the plane-wave Fourier transformation of the LMTOs in Ω_{int} has been implemented. So the charge density and the crystal potential have a dual representation: spherical harmonic expansions inside the spheres, R_{MT}, and plane-wave expansions in Ω_{int}. This is usually done by introducing a smooth pseudo-charge density $\tilde{\rho}$ over all space (the unit cell) via the pseudo-LMTOs. The pseudo-density coincides with the true charge density when $\boldsymbol{r} \in \Omega_{int}$.

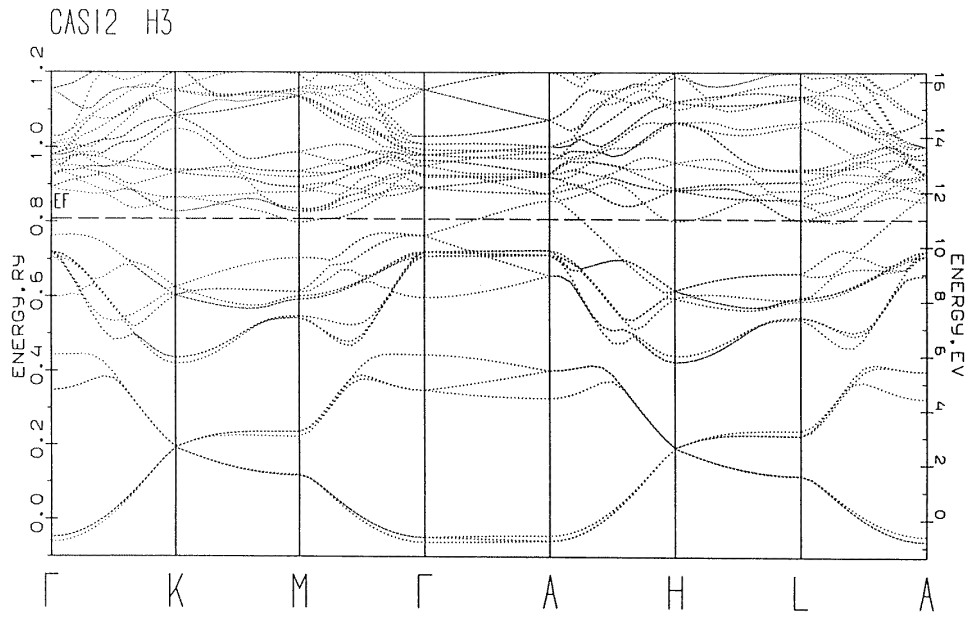

Figure 2. The band structure of H3-structure $CaSi_2$.

We use the double-κ spd LMTO basis set (18 orbitals per atom) with one-centre expansions inside the MT spheres performed up to $l_{max} = 6$. In the interstitial region, the s, p, d basis functions are expanded in plane waves up to 5.8, 8.27, 12.1 Ryd (328, 560, 920 plane waves) for Ca, and up to 14.0, 20.4, 30.0 Ryd (1230, 2130, 3784 plane waves) for Si. The charge densities and the potentials are represented inside the MT spheres by spherical harmonics up to $l_{max} = 6$, and by plane waves with a 50.04 Ryd energy cut-off (8102 PWs) in the interstitial region, which corresponds to the $(20, 20, 70)$ fast-Fourier-transform grid in the unit cell.

The $\boldsymbol{k}$-space Brillouin zone integrations needed for constructing the charge density (and potential) are performed over the $(16, 16, 5)$ grid (132 points per 1/24 irreducible part of the Brillouin zone) by use of an improved technique developed in [19]. The MT-sphere radius of Ca is taken to be 3.582 au and the radius of the silicon sphere is 2.276 au. In $CaSi_2$ the sphere radii are mainly determined by the Si–Si bond length (the shortest mutual distance between the constituents of $CaSi_2$) in the bilayers of Si between Ca layers.

We did not perform a full minimization of the total energy with respect to the volume and the internal displacement parameter z. For the TR3 and H3 crystal structures we have used the experimental in-plane lattice constant, $a = 3.82$ Å, the out-of-plane lattice constant, $c = 15.98$ Å, and the internal displacement parameter $z = 0.197$ [11]. For complex crystal structures it is important to control and manage the process of stabilization of the self-consistent iterations. For this purpose, the Broyden procedure [20] for mixing input and output electron and spin densities has been applied. It was found [21] that the use of this scheme significantly accelerates charge- (and spin-) density convergence. The latter was checked through the total energy, which was stable to within 0.1 μRyd in the last iterations towards the self-consistency.

It should be noted that our first calculation was done for the H1 structure with

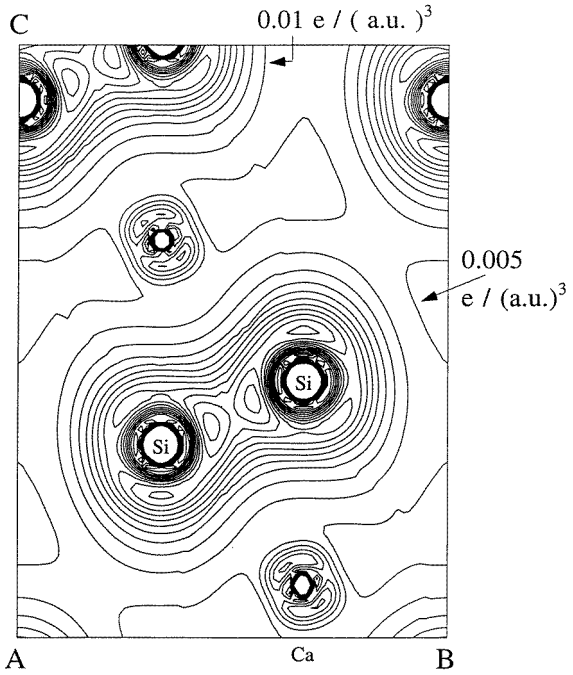

Figure 3. A contour plot of the charge density for the TR3 structure. The vertical direction is parallel to the *c*-axis. Equicharge contours are plotted in steps of 0.005 electrons au^{-3}. Points A, B and C have the following coordinates (in units of the lattice constant *a*): A: (0, 0, 0.63); B: $(3/2, \sqrt{3}/2, 0.63)$; C: (0, 0, 2.93).

1 f.u./primitive cell. The shape of band structure was very similar to that of Fahy and Hamann's dispersion curves (figure 4 in [8]).

4. The electronic structure of $CaSi_2$

Figures 1 and 2 show the calculated energy bands along high-symmetry directions in the hexagonal Brillouin zone for the TR3 and H3 structures, respectively, and show an obvious resemblance (except for details along the M–K and H–L lines), especially for the 14 fully filled bands below the Fermi level (E_F). There is a small difference between the states at E_F, reflecting the sensitivity of the Fermi surface topology to the stacking sequence. Higher conduction bands lying above E_F are somewhat more sensitive to stacking. It is seen that most bands have little dispersion in the Γ–A direction due to the strongly two-dimensional (uniaxial) layer structure of calcium disilicide.

A dramatic change occurs in the DOS at E_F that is double for the TR3 structure compared to the H3 one (cf. $N(E_F) = 30.22$ states Ryd^{-1}/cell for TR3 and 15.17 states Ryd^{-1}/cell for H3). An explanation of this large difference can be obtained by comparing the electron configurations of the Ca atom. Upon going from the TR3 to the H3 structure, the Ca d occupancy decreases (from 1.033 electrons to 0.873 electrons) and the accompanying upward shift of the Ca d band leads to strong variations of the DOS at E_F. Note that calcium has the s^2d^0 electronic configuration in the free atom. At the same time, the s and p occupancies of the Ca and Si atoms as well as the d occupancy of the Si atom, are

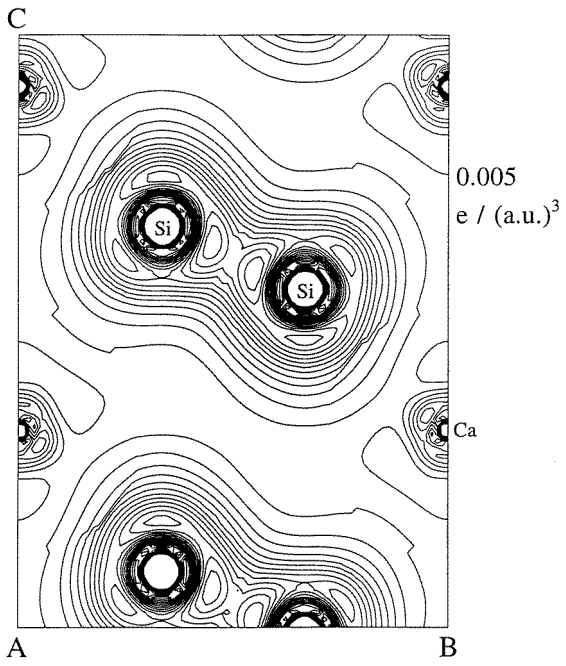

Figure 4. A charge-density contour plot for H3-structure $CaSi_2$, as in figure 3.

virtually unchanged in both the TR3 and H3 structures.

The difference in stacking sequence of the TR3 and H3 structures manifests itself in the spatial charge-density distribution, shown in figures 3 and 4. In the TR3 structure there is a tendency to form covalent bonds between the Ca atoms and the nearest Si layer, while in the H3 structure such a tendency is absent, though there is a very weak bond directed along the *c*-axis, which points from the Ca atom to the Si layer. At the same time, the Si–Si bond charges inside the Si double layers are similar for the two structures, and nearly the same as that for pure silicon. Note that for both structures TR3 and H3, in the basal plane (0001) containing the Ca atoms, the latter show an almost spherically symmetric distribution of the charge density. On the whole, one can say that for neither structure can one find noticeable bond orientation, and that the Ca layers interact weakly with the Si bilayers. Generally, our contour maps of the charge density for the TR3 structure coincide with Fahy and Hamann's data [8].

The origin of the various features present in the electronic structure can be studied by looking at the total and local (angular-momentum- and site-projected) DOS curves. These DOSs are displayed in figures 5 and 6 for the TR3 and H3 structures, respectively. The bands extending from about -0.05 Ryd to about 0.2 Ryd are primarily of silicon s parentage. There is a small gap at around 0.2 Ryd separating these from the p states of Si. Then we find states of varying intensity with mostly Ca spd character and Si p character which are highly hybridized. The Ca d character results from the lowering in energy of metal-derived 3d states which hybridize with Si-derived 3p states. This resulting p–d bonding combinations determine, generally, the stability of the compound.

Local DOS (LDOS) curves show that the change in stacking sequence produces a lowering of the Ca d bands upon going from the H3 to the TR3 structure too. This is due

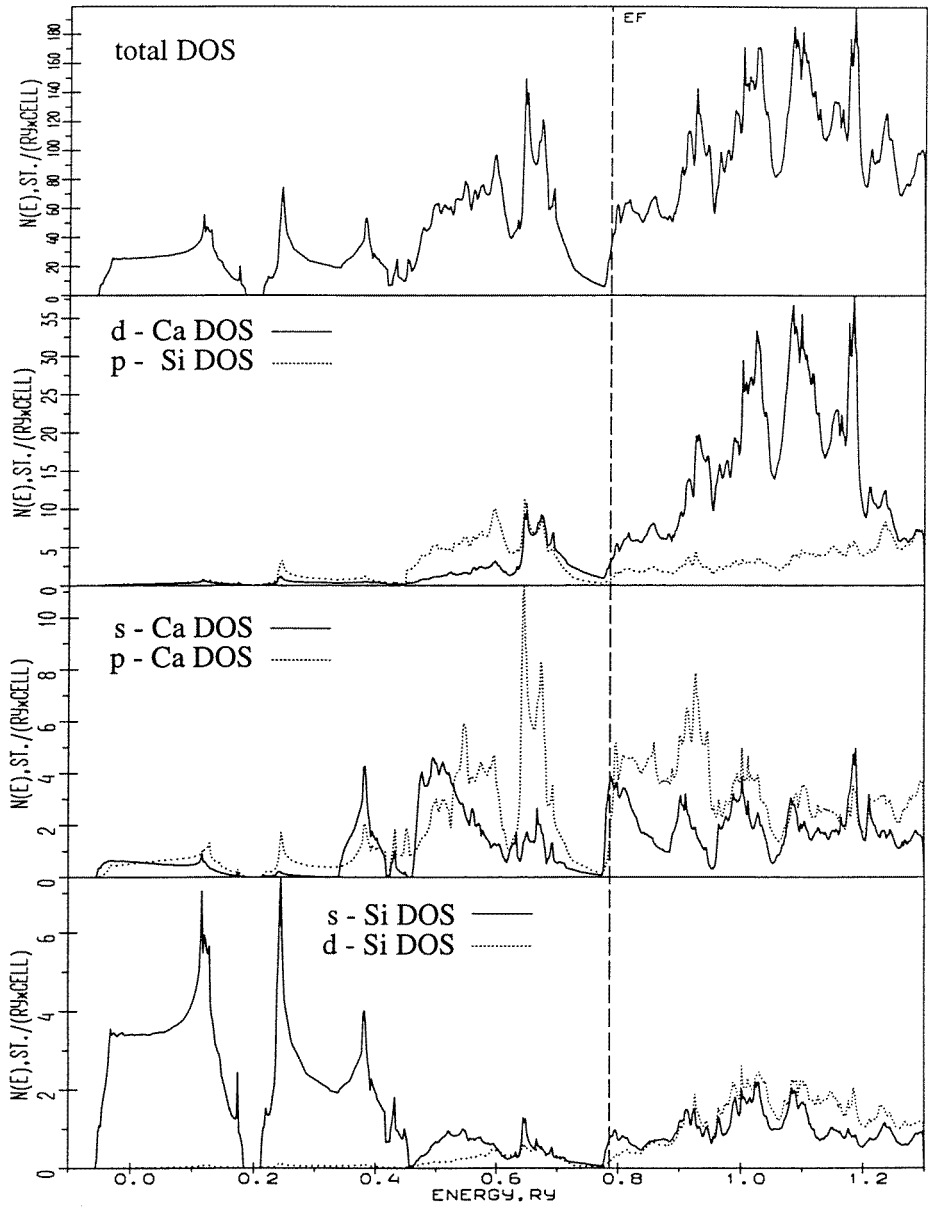

Figure 5. Total and local angular-momentum projected DOSs for the TR3 structure. The projections are per atom. The vertical dashed line denotes the Fermi level.

to the enhancement of the Ca–Si interaction (covalent mixing) which increases the Ca d occupancy. As a result, in the TR3 structure, the Ca d states below E_F do not belong to the tail of the unoccupied main d band, as in pure calcium, but form a bonding, well defined, structure separated from the empty d states. As seen from figure 5, the Ca spd and the Si sp states are hybridized to a large extent, and this bonding interaction is present at energies

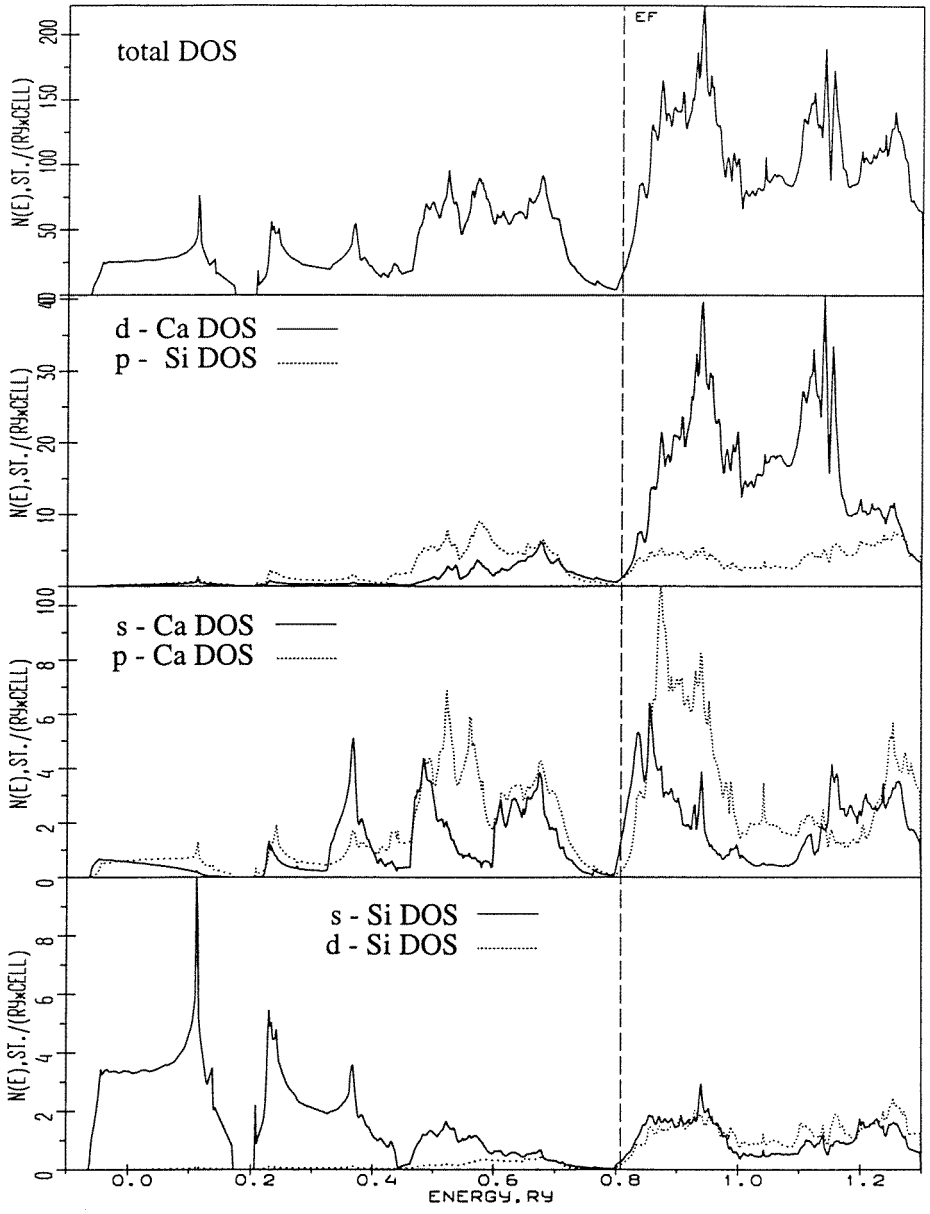

Figure 6. DOSs for H3-structure $CaSi_2$, as in figure 5.

from 0.46 Ryd up to E_F. There is steep increase for the Ca sp electronic states at the Fermi level. In this respect our results are in agreement with the earlier tight-binding results of reference [10] and disagree with the data of reference [8], in which the authors did not find any evidence of Ca 3p states near E_F.

The high-energy part of the DOS (or the empty states) is characterized by a broad Ca–Si structure which involves all of the Ca and Si electronic states. The main contribution to

the empty conduction band comes from the Ca d states. It should be noted that the Ca empty d-character DOS in the TR3 structure is a multipeaked curve, whereas it has only two features in the H3 structure. Below we will see how this difference in the final states is reflected in optical spectra.

The Fermi surface in the TR3 structure emerges from the two bands crossing E_F, the 15th and 16th, and consists of the small electron pockets near the M and L points, and the large hole pocket centred at the A point. The shape of the hole pocket is approximately ellipsoidal, whereas the shape of the electron pockets shows a large degree of dependence on the position of the Fermi level due to very flat Ca d bands near the M and L points. Hence, the effective masses of the electron carriers are much larger than those of the hole carriers.

5. Optical spectra

Our calculations of optical spectra are based on the widely used RPA-type expression for the interband absorptive part of the conductivity tensor (see, for example, reference [22]):

$$\sigma_{\alpha\beta}^{\mathrm{abs}}(\omega) = \frac{e^2\hbar^2}{m^2\omega\Omega}\sum_{i,f}\int \mathrm{d}\boldsymbol{k}\ p_\alpha^{if}(\boldsymbol{k})p_\beta^{fi}(\boldsymbol{k})f_i(\boldsymbol{k})[1-f_f(\boldsymbol{k})]\delta(\hbar\omega - E_{fi}(\boldsymbol{k})). \tag{1}$$

Here i and f refer to the initial and final relativistic band states, $E_{fi}(\boldsymbol{k}) = E_f(\boldsymbol{k}) - E_i(\boldsymbol{k})$, Ω is the unit-cell volume, $f_i(\boldsymbol{k})$ and $f_f(\boldsymbol{k})$ are occupation numbers for the initial and final states, $p_\alpha^{if}(\boldsymbol{k}) = \langle i\boldsymbol{k}|\hbar\nabla_\alpha/\mathrm{i}|f\boldsymbol{k}\rangle$ is the matrix element (ME) of the momentum operator in the dipole approximation, $\hbar\omega$ stands for the photon energy, and $\alpha, \beta = x, y, z$. The matrix elements for the transition between each pair of the occupied (initial) and empty (final) band states are calculated at each $\boldsymbol{k}$-point using the relativistic LMTO wave functions. The interband optical conductivity is then evaluated by considering all possible pairs of the direct (vertical) transitions, and is related to the imaginary part of the dielectric function $\varepsilon_{2,\alpha\alpha}$ through $\varepsilon_{2,\alpha\alpha}(\omega) = (4\pi/\omega)\sigma_{1,\alpha\alpha}(\omega)$. Generally, the complex tensors $\boldsymbol{\varepsilon}(\omega)$ and $\boldsymbol{\sigma}(\omega)$ are related by the following equation: $\varepsilon_{\alpha\beta}(\omega) = \delta_{\alpha\beta} - \mathrm{i}(4\pi/\omega)\sigma_{\alpha\beta}(\omega)$. The dissipative part of the conductivity tensor $\sigma_{2,\alpha\alpha}(\omega)$ has been calculated from the Kramers–Kronig transformation in the energy interval 0–21.8 eV.

The intraband part of the diagonal components of the conductivity tensor can be found by use of the conventional Drude formula (see, for example, reference [23]):

$$\sigma_{\alpha\alpha}^{\mathrm{intra}}(\omega) = \frac{\omega}{4\pi}\left(1 - \frac{\omega_p^2}{\omega(\omega+\mathrm{i}\gamma)}\right) \tag{2}$$

where

$$\omega_p^2 = \frac{4\pi e^2 m}{\hbar\Omega}\sum_i\int \mathrm{d}\boldsymbol{k}\ \delta(E_i(\boldsymbol{k}) - E_F)(\nabla_{k\alpha}E_i(\boldsymbol{k}))^2$$

where $(\nabla_{k\alpha}E_i(\boldsymbol{k}))^2 = {v_{k\alpha}}^2$ and ω_p^2 is the Drude plasma frequency. From the calculated Fermi velocities ($v_{F,\alpha}$), the averaged basal-plane and zz-components of the Drude plasma frequency have the values 3.02 eV and 1.21 eV, respectively, for the TR3 structure, and 1.99 eV and 1.97 eV for the H3 structure. Since the density functional theory has been implemented to produce electronic spectra of the ground-state properties, using the LDA bands to calculate the quasiparticle velocities is an approximation. However, the validity of this approximation has been proved to be reliable for non-magnetic metals and compounds in a number of LDA Drude plasma frequency calculations [24, 25].

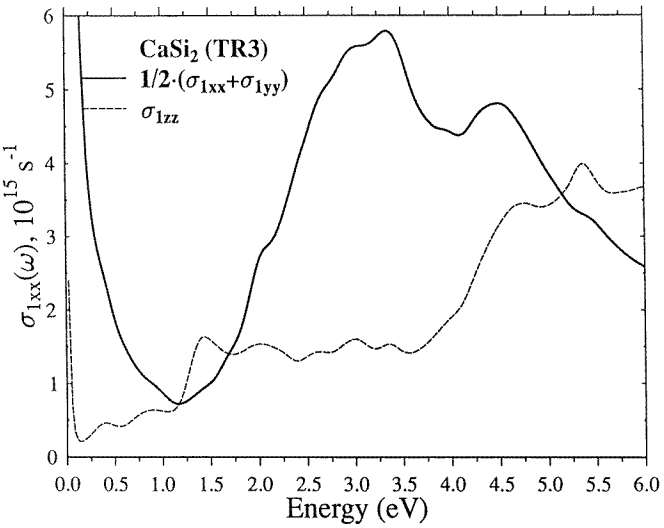

Figure 7. Calculated absorptive diagonal components of the conductivity tensor in the basal plane (solid line) and along the *c*-axis (dashed line) for the TR3 structure.

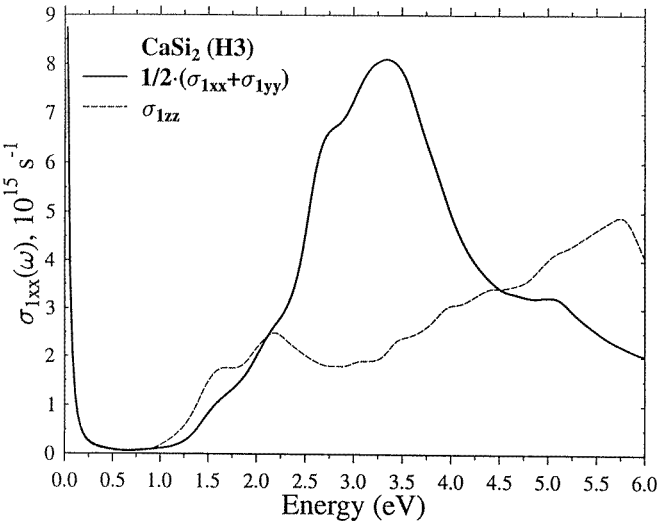

Figure 8. Absorptive diagonal components of the conductivity tensor for H3-structure $CaSi_2$, as in figure 7.

For metals, the scattering rate γ is determined by the electron–phonon interaction, and can be found from the electroresistivity ρ at the Debye temperatures by use of an expression from [23]: $\gamma = 4\pi\omega_p^2\rho$. We used data on ρ at room temperature from [13]. So, the scattering rate γ is the only phenomenological parameter used in our optical calculations.

Other optical characteristics may be obtained from the dielectric function—for example, the reflectivity $R(\omega)$ and the electron energy-loss spectrum EELS(ω), which determines the

energy loss of the fast electrons passing through the films:

$$R(\omega) = \left| \left(\frac{\sqrt{\varepsilon(\omega)} - 1}{\sqrt{\varepsilon(\omega)} + 1} \right)^2 \right| \qquad \mathrm{EELS}(\omega) = \mathrm{Im}\left[-\frac{1}{\varepsilon(\omega)} \right]. \tag{3}$$

Our band-structure and optical calculations have been carried out by the linear muffin-tin orbital (RLMTO–ASA) method [14, 22] using scalar relativistic MT orbitals and including spin–orbit coupling (SOC) in the variational procedure, which implies that the SOC Hamiltonian is diagonalized using the spin-polarized scalar relativistic wave functions as a basis set. Because of the weakness of the SOC compared to the crystal-field and exchange splittings, especially for $CaSi_2$, such a perturbative procedure is justified. In the iterations towards self-consistency of the single-particle effective crystal potential, the exchange splitting and the SOC are considered on an equal footing, i.e. both of these terms are effective in the formation of the potential.

In calculations for the H3 and TR3 structures (the self-consistent electronic structure and the conductivity tensor) we used the same grid of 306 $\boldsymbol{k}$-points in the 1/24 irreducible part of the hexagonal Brillouin zone, whereas the basis functions were s, p, d, f LMTOs for the Ca atom and s, p, d LMTOs for the Si atom. The ratios of the ASA radii were taken as $S^{\mathrm{Ca}}/S^{\mathrm{Si}} = 1.25$. This choice has provided a very small charge transfer between the Ca and Si sites, equal to 0.02. To check the optimal sphere radii ratio, we used a contour map of the charge-density distribution obtained by the full-potential LMTO–PW method (see figure 3). The minimum of the electron density along the Ca–Si direction occurs at the point which divides the Ca–Si spacing in a ratio of about 1.2:1.0. This proves that our choice of sphere radii ratio for $CaSi_2$ is correct. The RLMTO–ASA electronic structure and DOS curves obtained are similar to those from the FPLMTO–PW method except for details, as here we use the SOI contributions which remove the accidental band crossings inside the valence band and the degeneracies at the top of the Brillouin zone (the AHL plane) except for the A–L line. As a result of such modification of the electronic structure, the width of the valence and conduction bands and the DOS at E_{F} slightly increase in comparison with those for the scalar relativistic FPLMTO–PW band structure.

Calculations of the interband absorptive part of conductivity tensor have been made using equation (1). In addition, we smooth the conductivity tensor using the constant inverse lifetime $\Gamma(\omega)$ = 0.1 eV (a so-called Lorentz convolution), and add the intraband Drude contribution, equation (2), to the interband diagonal components of the conductivity tensor.

Figures 7–10 represent our calculated $\sigma_{1,\alpha\alpha}(\omega)$, $R(\omega)$ and $\mathrm{EELS}(\omega)$ spectra (equation (3)) for the TR3 and H3 structures, respectively. Interband direct transitions start at very small photon energy (0.02 eV) in the TR3 structure whereas in the H3 structure an absorption edge of about 0.35 eV is found. Figures 7 and 8 show that the conductivity spectra have a pronounced extremum at 3.3 eV for the in-plane conductivity. The out-of-plane conductivity ($\sigma_{1,zz}$) is about four times smaller at this photon energy. The anisotropy of $\sigma_{1,\alpha\alpha}(\omega)$ for $CaSi_2$ is a consequence of uniaxial crystal structure. Also it is seen that the conductivity in the TR3 structure has the additional features at 4.5 eV and 5.3 eV which are absent for the H3 structure. This finding is in agreement with the above-mentioned analysis of the empty (final) states in the TR3 and H3 structures.

The energy dependence of the reflectivity in the infrared region in the TR3 and H3 structures is quite different (figures 9 and 10). In the H3 structure a sharp drop of $R(\omega)$ occurs at $\hbar\omega = 0.6$ eV (the transition to the transmittance regime), accompanying the strong plasma peak. In the TR3 structure the plasma peaks are damped in amplitude and shifted in energy for the basal-plane and zz-directions, and here $R(\omega)$ resembles that for ordinary

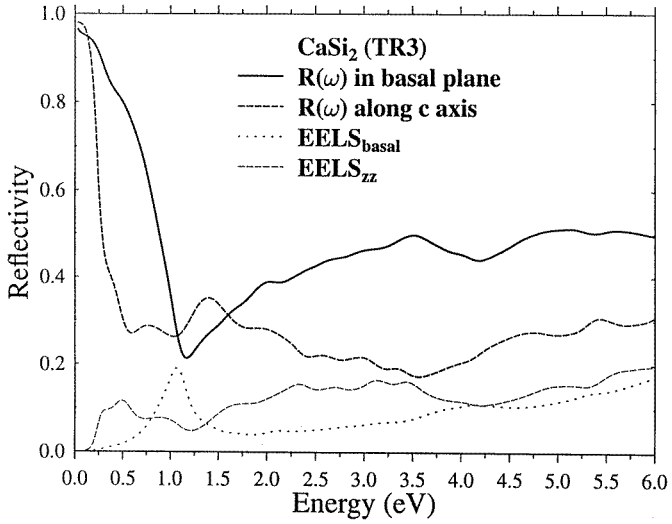

Figure 9. Calculated spectra of the reflectivity and EELS for TR3-structure $CaSi_2$.

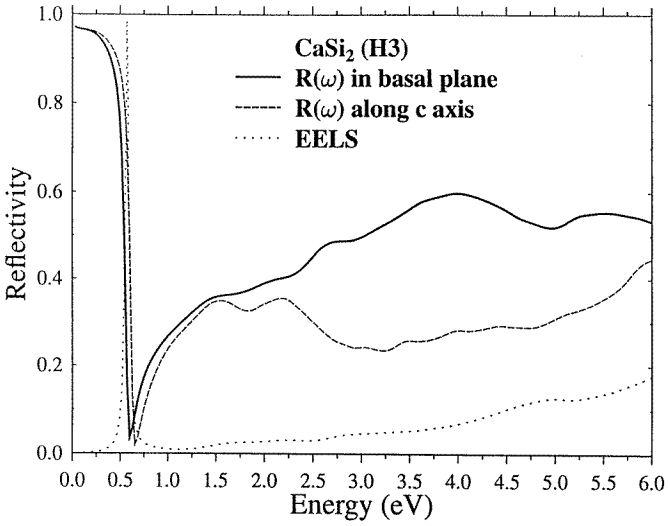

Figure 10. Calculated spectra of the reflectivity and EELS for the H3 structure.

transition metals.

Finally, by use of our calculated Fermi velocities (or, equivalently, the plasma frequencies) it is possible to carry out a qualitative analysis of the transport properties. $CaSi_2$ is metallic, and the electrical resistivity ranges between 19.5 and 25.5 $\mu\Omega$ cm at 4.2 K, depending on the crystal orientation [26]. From an approximate variational solution of the Boltzmann equation, ρ can be expressed as $\rho = (N(E_F)v_F^2)^{-1}\pi\Omega_{cell}k_BT\lambda_{e-ph}$. The Fermi velocities in the H3 structure are isotropic whereas in the TR3 structure those in the basal plane are larger by one order of magnitude than those along the *c*-axis. This implies a significant orientation dependence of the transport properties for the TR3 structure. The

fact that almost no resistivity anisotropy was measured [26] may mean that the authors have used the TR6 phase of $CaSi_2$ and that there were random distributions of uniaxial domains or twins in their sample.

6. Summary

In summary, we have studied the electronic and optical spectra of the experimentally observed TR3 structure and of the hypothetical H3 one, i.e. for two different stacking sequences. We have found that the difference in stacking sequence manifests itself in the spatial charge-density distributions. Drastic changes occur also at the Fermi level. As a result, in the TR3 structure, the DOS at E_F is twice that of the H3 structure. The optical spectra in the infrared region are quite different for the TR3 and H3 structures due to the different spatial distributions of the Fermi velocities in the two structures.

Acknowledgments

The authors are grateful to Dr S Savrasov for providing us with the FPLMTO–PW program and Mr T Arioka for technical assistance. The computations were performed at the Information Processing Centre of Kobe University. One of us (EK) acknowledges financial support from the Photonics Materials Laboratory Project of the Venture Business Laboratory of Kobe University.

References

[1] Takeda K and Shiraishi K 1989 *Phys. Rev.* B **39** 11 028
[2] Deak P, Rosenbauer M, Stutzmann M, Weber J and Brandt M S 1992 *Phys. Rev. Lett.* **69** 2531
[3] Fuchs H D, Stutzmann M, Brandt M S, Rosenbauer M, Weber J, Breitschwerdt A, Deak P and Cardona M 1993 *Phys. Rev.* B **48** 8172
[4] Abe S, Nakayama H, Nishino T and Iida S 1997 *Appl. Surf. Sci.* **113/114** 562
[5] Abe S, Nakayama H, Nishino T and Iida S 1997 *J. Mater. Res.* **12** 407
[6] Sancrotti M and Rizzi A 1988 *Phys. Rev.* B **37** 3120
[7] Calliari L, Marchetti F, Sancrotti M, Bisi O, Iandelli A, Olcese G L and Palenzona A 1990 *Phys. Rev.* B **41** 7569
[8] Fahy S and Hamann D R 1990 *Phys. Rev.* B **41** 7587
[9] Bisi O, Braicovich L, Carbone C, Lindau I, Iandelli A, Olcese G L and Palenzona A 1989 *Phys. Rev.* B **40** 10 194
[10] Xu Yongnian, Zhang Kaiming and Xie Xide 1986 *Phys. Rev.* B **33** 8602
[11] Janzon K H, Schafer H and Weiss A 1968 *Z. Naturf.* b **23** 1544
[12] Evers J 1979 *J. Solid State Chem.* **28** 369
[13] Hirano T and Fujiwara J 1991 *Phys. Rev.* B **43** 7442
[14] Andersen O K 1975 *Phys. Rev.* B **12** 3060
[15] Savrasov S Y 1996 *Phys. Rev.* B **54** 16 470
[16] von Barth U and Hedin L 1972 *J. Phys. C: Solid State Phys.* **5** 1629
[17] Hohenberg P and Kohn W 1964 *Phys. Rev.* **136** B864
[18] Kohn W and Sham L J 1965 *Phys. Rev.* **140** A1133
[19] Bloechl P, Jepsen O and Andersen O K 1994 *Phys. Rev.* B **49** 16 223
[20] Johnson D D 1988 *Phys. Rev.* B **38** 12 807
[21] Kulatov E and Ohta H 1997 *J. Phys. Soc. Japan* **66** 2386
[22] Uspenskii Y A, Kulatov E T and Halilov S V 1996 *Phys. Rev.* B **54** 474
[23] Mazin I I, Savitskii E M and Uspenskii Yu A 1984 *J. Phys. F: Met. Phys.* **14** 167
[24] Allen P B 1987 *Phys. Rev.* B **36** 2920
[25] Leung Chinmong, Weinert M, Allen P B and Wentzcovitch R M 1996 *Phys. Rev.* B **54** 7857
[26] Hirano T 1991 *J. Less-Common Met.* **167** 329